






Research Article

A Simple Method to Produce an Aluminum Oxide-Passivated Tungsten Diselenide/n-Type Si Heterojunction Solar Cell with High Power Conversion Efficiency

Malik Abdul Rehman,^{1,2} Minjae Kim ,¹ Sachin A. Pawar,³ Sewon Park,⁴ Naila Nasir,⁵ Dong-eun Kim ,¹ Muhammad Farooq Khan,⁶ Van Huy Nguyen,⁵ Akendra Singh Chabungam ,¹ Yongho Seo,⁵ Takeaki Sakurai,³ Seung-Hyun Chun,⁷ Do Hyoung Koo,⁸ Chul-Ho Lee,⁸ Seong Chan Jun ,⁴ and Hyung-Ho Park ¹

¹Department of Materials Science and Engineering, Yonsei University, Seoul 03722, Republic of Korea

²Department of Chemical Engineering, New Uzbekistan University, Tashkent, Uzbekistan

³Department of Applied Physics, Faculty of Pure and Applied Sciences, University of Tsukuba, Tsukuba, Ibaraki 305-8573, Japan

⁴Nano-Electromechanical Device Laboratory, School of Mechanical Engineering, Yonsei University, Seoul 03722, Republic of Korea

⁵Department of Nanotechnology and Advanced Materials Engineering and HMC, Sejong University, 05006 Seoul, Republic of Korea

⁶Department of Electrical Engineering, Sejong University, Seoul 05006, Republic of Korea

⁷Department of Physics and Astronomy, Sejong University, Seoul 05006, Republic of Korea

⁸KU-KIST Graduate School of Converging Science and Technology, Korea University, Seoul 02841, Republic of Korea

Correspondence should be addressed to Seong Chan Jun; scj@yonsei.ac.kr and Hyung-Ho Park; hhpark@yonsei.ac.kr

Received 3 September 2022; Revised 4 December 2022; Accepted 6 December 2022; Published 23 February 2023

Academic Editor: Soumyendu Roy

Copyright © 2023 Malik Abdul Rehman et al. This is an open access article distributed under the Creative Commons Attribution License, which permits unrestricted use, distribution, and reproduction in any medium, provided the original work is properly cited.

Transition metal dichalcogenide (TMDC) materials are attractive candidates for 2D solar cell devices thanks to their straightforward integration with various substrates and traditional semiconductor technologies, wide band gap ranges over the visible light spectrum, and high absorption coefficient values. Although there are several previous reports on the fabrication of 2D material-based solar cells, difficult and complex processes in the fabrication are highly required to be modified for wider use in daily life applications. Photolithography, the most commonly used manufacturing process for TMDC-based solar cells, is complicated. In this study, we demonstrate that the fabrication of 2D tungsten diselenide (WSe_2) by adopting a wet transfer process with thermal release tape simplifies the manufacturing steps for TMDC-based solar cell devices. This simplification not only reduces the production cost by excluding several factors such as transmittance, thermal expansion, surface flatness, and durability but also improves the yield. Furthermore, a proof-of-concept demonstration of creating a WSe_2/Si junction with an aluminum oxide (Al_2O_3) antireflective coating provided a power conversion efficiency of 6.39%, which is a significant improvement over that of a WSe_2/Si solar cell without the antireflective coating layer (1.08%).

1. Introduction

The earth's temperature is slowly increasing owing to global warming caused by the enormous dependence of humans on fossil fuels as energy sources. In the process of maintaining carbon dioxide (CO_2) at a relatively safe level to avoid environmental catastrophe, alternative energy sources that are

clean, green, reliable, and free from carbon are highly desirable. Highly abundant solar energy is the most dependable and potent renewable energy option [1–4], and making solar cells to harness it that are highly efficient and affordable is key to tackling the continuously increasing energy demand around the globe. Efforts are ongoing in the research community to develop cheap photovoltaics with practicable

power conversion efficiency (PCE) levels. However, these efforts are being hindered by various limitations in the fabrication, selection, stability, and affordability of photovoltaic materials [5, 6].

Graphene, a zero-band gap material, is incapable of electrically driven light emission. On the other hand, transition metal dichalcogenides (TMDCs) have drawn much attention for use in various optoelectronic, 2D solar cell, energy conversion, and storage applications owing to their layered nature and tunable thickness-dependent band gap energy levels [7–11]. Solar cells that are only a few layers comprising 2D TMDCs with van der Waals junctions have shown outstandingly high photocurrent levels. In recent years, 2D MXenes have also drawn interest in the field of photovoltaics as electron transport layer for their distinctive properties such as metallic conductivity and tunable work function for improving the device efficiency and stability [12, 13]. Moreover, compared to existing solar cells, they have comparatively higher chemical stability and require less material, leading to a cost reduction in their fabrication [14].

Due to their band gap energy and thickness-dependent behavior, 2D materials such as molybdenum disulfide (MoS_2) and tungsten diselenide (WSe_2) have recently gained noteworthy attention as materials for making solar cells. MoS_2 and WSe_2 monolayers have a direct band gap while their bulk forms can be used to produce indirect semiconductors [1, 4, 15–18]. Among the TMDCs for solar cells, tungsten diselenide (WSe_2) is the most promising candidate mainly due to its bulk band gap energy of ~ 1.3 eV. The Shockley-Queisser detailed balance limit provides the maximum photoconversion efficiency for a single absorber comprising WSe_2 . Moreover, WSe_2 possesses a high absorption coefficient of 10^5 cm^{-1} at 780 nm and high electron and hole carrier mobility ($>100 \text{ cm}^2/\text{V s}$) [19, 20].

WSe_2 has been used as an absorber in intriguing 2D solar cell investigations [21, 22]. However, the ones with a sufficiently high PCE have not yet been achieved and have failed to meet the theoretical PCE range of 20–27%. Thus, it is highly desirable to more effectively exploit TMDCs in solar cells, especially WSe_2 considering its electronic properties, passivation effect, durability, and use as a counter electrode [23–25]. Al_2O_3 with a band gap of ~ 8.3 eV is well known for its superior dielectric, thermal stability, and excellent adhesion to other materials. Due to its ability to increase intrinsic potential and reduce recombination, Al_2O_3 serves as an electron blocking layer and a passivating layer for silicon surfaces. Moreover, Al_2O_3 film helps in decreasing the leakage current which restricts the insulating characteristics that impacts the efficiency of the device. Large built-in fields are produced as a result of lower reflection losses due to the Al_2O_3 layer and an increase in photons trapped inside the depletion area.

In this study, we explored a WSe_2/n -type Si heterojunction solar cell and the effect of aluminum oxide (Al_2O_3) passivation on its PCE. A large area of WSe_2 was grown via chemical vapor deposition (CVD) and simply wet transferred with thermal release tape (TRT) to produce a WSe_2 film that is a few layers thick. In addition, we fabricated a WSe_2/n -type Si heterojunction solar cell with Au fingers as the top contact and Ti/Pd/Ag as the bottom contact. An

Al_2O_3 antireflective and passivating layer was coated on the device by using atomic layer deposition (ALD). The CVD-grown WSe_2 was atomically thin. The photovoltaic performance of the WSe_2/n -type Si heterojunction solar cell with an Al_2O_3 passivating layer under air mass (AM) 1.5 was obtained. Al_2O_3 surface passivation, band alignment between WSe_2 and n -type Si, and PCE improvement in the WSe_2/n -type Si-enabled heterojunction solar cell due to the Al_2O_3 passivating layer were also investigated. The thickness of the prepared Al_2O_3 interfacial layer is around 10 nm. The purpose of using 10 nm thickness is to improve the trap density of deteriorated $\text{Al}_2\text{O}_3/\text{WSe}_2$ interface [26]. As reported in previous reports, the 10 nm thickness of Al_2O_3 will help in the suppression of the Coulomb scattering, thereby modifying the dispersion of phonons. Moreover, the growth of ALD is helpful in removing the impurities, and due to the difference in the dielectric constant of silicon and Al_2O_3 , therefore passivation layer using Al_2O_3 significantly improves the solar cell device efficiency [27–29].

2. Experimental

2.1. Wafer-Scale Growth of WSe_2 . The growth of WSe_2 was carried out in a 2-inch vertical cold-wall chamber. Tungsten hexacarbonyl (THC, $\text{W}(\text{CO})_6$) and diethyl sulfide (DES, $(\text{C}_2\text{H}_5)_2\text{Se}$) as the W and Se precursors, respectively, in the gaseous phase were injected into the chamber. We maintained THC used for growth at 0°C , DES at -15°C , and grew WSe_2 in vapor phase form using Ar gas. Ar and H_2 were also injected into the chamber to deliver and react with the W and Se precursors, respectively. The optimized experimental conditions to produce WSe_2 films were a total pressure of 50 Torr, a growth temperature of 600°C , and a growth time of 130 min. Ar gas that goes directly into the source flowed 10 sccm in the case of THC and 3 sccm in the case of DES. Also, the dilution gas to adjust the flow rate was 50 sccm and 57 sccm, and the total amount flowed to 60 sccm.

The flow rates of the precursors were 10 and 3 sccm for THC and DES, respectively, which increased to 60 and 5 sccm by adding Ar and H_2 gas, respectively.

2.2. Cleaning Process of n -Type Si. n -type, (100)-oriented bare polished native oxide (SiO_2) was doped with phosphorous with resistivity ranging from 1 to $10 \Omega\text{cm}$. The removal of heavy residues was achieved by cleaning the Si substrates using warm (55°C) trichloroethylene (TCE), acetone, methanol, and deionized (DI) water.

2.3. Transferring the WSe_2 Film onto an n -Type Si Substrate. A 100 nm thick polymethyl methacrylate (PMMA) layer was deposited onto $\text{WSe}_2/\text{SiO}_2$ samples via spin coating at 3000 rpm for 45 s. To obtain a PMMA/ WSe_2 stack, the PMMA/ $\text{WSe}_2/\text{SiO}_2$ substrate was placed in buffered oxide etch solution for 3 h to etch the SiO_2 . After wet etching, the PMMA/ WSe_2 stack transformed the SiO_2 substrate into an n -type Si substrate. The PMMA/ WSe_2/n -type Si sample was dried in a glove box in a vacuum ($<2 \times 10^{-2}$ Torr) for 24 h. After drying, it was immersed in acetone for 3 h to remove the PMMA and annealed in an Ar atmosphere at

350°C for 4 h to remove the polymer residues and contaminants. The front electrodes were made of metal grid finger bars, and the WSe₂/n-type Si with TRT was affixed at the edge to avoid the Schottky contact of the metal with Si. Although the metal grid bars were larger than the WSe₂ film, the size of the device was adjusted by using TRT. The TRT was easily removed by heating to 120°C, and Cr (10 nm)/Au (90 nm) was deposited on the front (emitter) side of the electrodes by using an e-beam evaporator at a base pressure of 1×10^{-6} Torr and a deposition rate of $\sim 1.6 \text{ nm s}^{-1}$. Afterward, an e-beam evaporator was used to deposit Ti (5 nm)/Pd (5 nm)/Ag (400 nm) on the back side of the electrodes to ensure low contact resistance.

2.4. Fabrication of the Al₂O₃ Antireflective Layer. A traveling wave type Lucida D100 system (NCD Tech, Inc., Korea) was used to deposit an antireflective Al₂O₃ layer on the Si substrate at 170°C. Trimethylaluminum (TMA; Ezchem Co., Ltd., Korea) was used as the Al source and DI water as the O source. Exceptionally pure N₂ carrier gas (99.999%) at a flow rate of 20 sccm was used to carry the respective sources into the reaction chamber. The antireflective Al₂O₃ layer was grown by using the following ALD precursor pulse and purge procedure: TMA pulse (0.1 s) → N₂ purge (8 s) → H₂O pulse (0.1 s) → N₂ purge (8 s).

2.5. Characterization Tools and Photovoltaic Measurements. The electronic structure of WSe₂ was determined by using the Raman spectroscopy (Renishaw in-Via, 514.5 nm wavelength). With a spot size of around 0.8 μm, a modest input power of 1 mW was employed to prevent any laser-related device damage. Measurements were taken at several locations, and the average findings were calculated to ensure the consistency and correctness of the data derived from each sample. The thickness of the WSe₂ layer was examined via atomic force microscopy (AFM; MultiMode 8, Bruker, USA). The WSe₂ elemental composition was determined by using X-ray photoelectron spectroscopy (XPS; K-alpha, Thermo UK) with an Al K monochromator (1486.6 eV) and a variable spot size (30–400 μm). A cross-sectional view of the WSe₂ film surface was verified by using high-resolution transmission electron microscopy (TEM; JEOL, JEM-F200). A UV-vis-near-IR spectrophotometer was exploited to capture optical reflectance spectra in the 200–900 nm region (V-750, JASCO). The photovoltaic performance of the device was measured by using a source meter in a solar simulator (1 sun power: Newport) (Keithley 2400). The system was calibrated with test samples before taking experimental measurements.

3. Results and Discussion

Figures 1(a) and 1(b) show flow charts of the conventional photolithography-based and new wet transfer with TRT-based methods for fabricating a p-n heterojunction solar cell, respectively, in which it can be seen that the new process is much simpler. Au and Al₂O₃ are two of the most crucial parameters in the device. Al₂O₃ was used as an antireflective layer of van der Waals (VDW) heterojunction-based p-n

junction solar cell formed by the p-type WSe₂ and n-type silicon contact. Therefore, Al₂O₃ was not deposited on top of Au contact as shown in Figure 2(a). It is critically essential that the depleted region of the VDW heterojunction device can separate the photoinduced charge carriers rapidly. The charges have been separated due to the creation of a built-in field and simultaneously collected at the top and bottom electrodes. The effective separation of photogenerated electron-hole pairs will create large built-in fields which are highly desirable to generate large photocurrents; therefore, it improves the efficiency of a solar cell. However, there are certain elements that degrade the performance such as inevitably inducing interface defects causing high recombination rate and lower built-in fields. Another important parameter is the illumination of solar simulator light which creates photons that must be absorbed in the depletion region rather than in the charge-neutral region in order to reduce the recombination of photogenerated electron-hole pairs [30]. Therefore, we have created two types of structures with and without Al₂O₃. In this case, without Al₂O₃, fewer photons are trapped within the depletion region and have a lower lifetime that resulted in large leakage currents and lower efficiency. However, with Al₂O₃, the reflection losses are reduced, and more photons are trapped within the depletion region, creating large built-in fields. McVay et al. [3] produced a WSe₂ solar cell device with a PCE of 0.96% by using a photolithography method. In the present research, we can confirm that removing the photoresist step not only simplifies the fabrication process but also solves the problem of residual chemicals, etc., and has a good effect on improving the performance of the device [31, 32]. The unique approach was adopted to fabricate solar cell devices without using the complicated lithography process and still producing a large active area that is essential from an industrial perspective. Figure 1(c) presents a schematic of the new simple fabrication process of a WSe₂/Si heterojunction by exploiting the wet transfer method.

Figures 2(a) and 2(b) show a schematic and a photograph of the device, respectively. Ti/Pd/Ag serves as the bottom electrode. It is widely recognized that the open-circuit voltage (V_{oc}) of solar cell devices is governed by the difference between the work function values of the bottom electrode and the absorber semiconductor layer [33–35]. The absorbent layer with Au fingers on top of the solar cell device is served by the WSe₂ layer created and transferred by using CVD. Finally, protection was achieved through coating with an Al₂O₃ passivating and antireflective layer grown by using ALD. The wet transfer process with TRT enabled the realization of a WSe₂/n-type Si heterojunction solar cell. The WSe₂ film was a few layers thick.

The morphological features of WSe₂ after being transferred to an n-type Si substrate were assessed by using high-resolution TEM and high-angle annular dark field-(HAADF-) scanning TEM (STEM). Figures 2(c) and 2(d) present the bilayer feature of the 2D WSe₂ film. Energy-dispersive X-ray spectroscopy (EDX) elemental mapping analysis identified the presence of W and Se from WSe₂ (Figures 2(e)–2(g)).

An AFM image of CVD-grown WSe₂ and the corresponding height profile to determine its thickness ($\sim 1.5 \text{ nm}$) are shown in Figures 3(a) and 3(b), respectively.

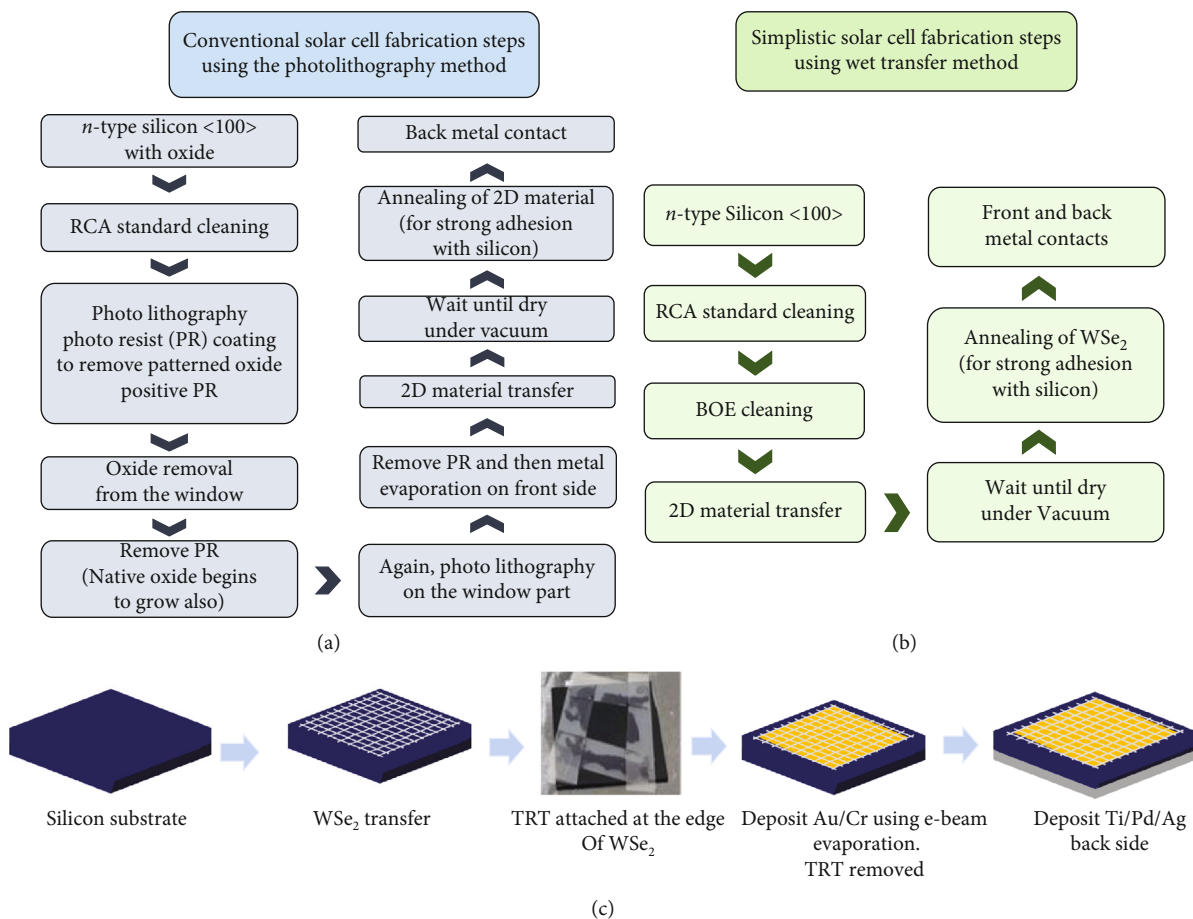


FIGURE 1: Flow charts of the WSe_2/Si heterojunction solar cell fabrication using (a) the conventional photolithography method and (b) the new simple fabrication process with the wet transfer method. (c) A schematic of the new simple fabrication process.

The thickness of the WSe_2 film indicates a multilayered structure, which is in accordance with the high-resolution TEM analysis. The thickness of the 2D WSe_2 is ~ 1.5 nm which can be predicted from the TEM image as shown in Figure 2(c). One more piece of evidence of multilayer has also been predicted from the Raman results.

Confirmation of the presence and structure of WSe_2 was performed by utilizing the Raman spectroscopy. The CVD-grown WSe_2 produced 2H phase active in-plane W-Se vibrational mode E_{2g}^1 [36]. The characteristic Raman peak at ~ 251 cm^{-1} with a shoulder at ~ 262 cm^{-1} attributed to in-plane vibrational mode E_{2g}^1 and out-of-plane vibrational mode A_{1g} , respectively [37–39], is indicative of the formation of multilayers of WSe_2 . Figure 3(c) shows the Raman spectra of WSe_2 before and after transfer. The spectrum after transfer has an extra peak at 304 cm^{-1} assigned to the B_{2g}^1 mode arising from interlayer interactions, which distinguishes multilayer WSe_2 from monolayer WSe_2 [40].

The top layer of solar cells must have zero reflection while that of the back surface must be maximized for the absorber layer to absorb as much sunlight as possible, resulting in a high photocurrent. Figure 3(d) shows optical reflectance spectra for n-type Si, $\text{WSe}_2/\text{n-type Si}$, and $\text{Al}_2\text{O}_3/$

$\text{WSe}_2/\text{n-type Si}$. The reflectance of $\text{Al}_2\text{O}_3/\text{WSe}_2/\text{n-type Si}$ was lower than the others, indicating higher absorbance that would result in higher photocurrent. As we have shown in Figure 3(d), the n-type polished silicon has very high reflectance $\sim 55\%$ at the visible portion 400 nm to 700 nm and even reflectance is significantly increased at below wavelength in the near-infrared region. However, in the case of ARC, the reflectance is significantly reduced to $\sim 35\%$ which also gives a piece of evidence; the absorption of photons is particularly increased. Therefore, an enhanced amount of photogenerated electrons will reduce the leakage current, and more charge carriers will be collected at the electrodes.

The chemical composition and valence states of WSe_2 were analyzed by using XPS (Figure 4). The W 4f XPS spectrum for WSe_2 in Figure 4(a) revealed peaks located at 34.38 eV and 32.28 eV deconvoluted into W $4f_{5/2}$ and W $4f_{7/2}$, respectively, while the Se 3d XPS spectrum for WSe_2 in Figure 4(b) shows peak located at 54.58 eV and 55.38 eV deconvoluted into Se $3d_{3/2}$ and Se $3d_{5/2}$, respectively. The pair of peaks for W $4f_{5/2}$ and W $4f_{7/2}$ at binding energies of 35.58 eV and 37.58 eV, respectively, are from WO_3 arising from the oxidation of WSe_2 exposed to air, which is a commonly observed phenomenon [36, 41]. Similarly, the W 4f XPS spectrum for $\text{Al}_2\text{O}_3/\text{WSe}_2$ in Figure 4(a) shows that

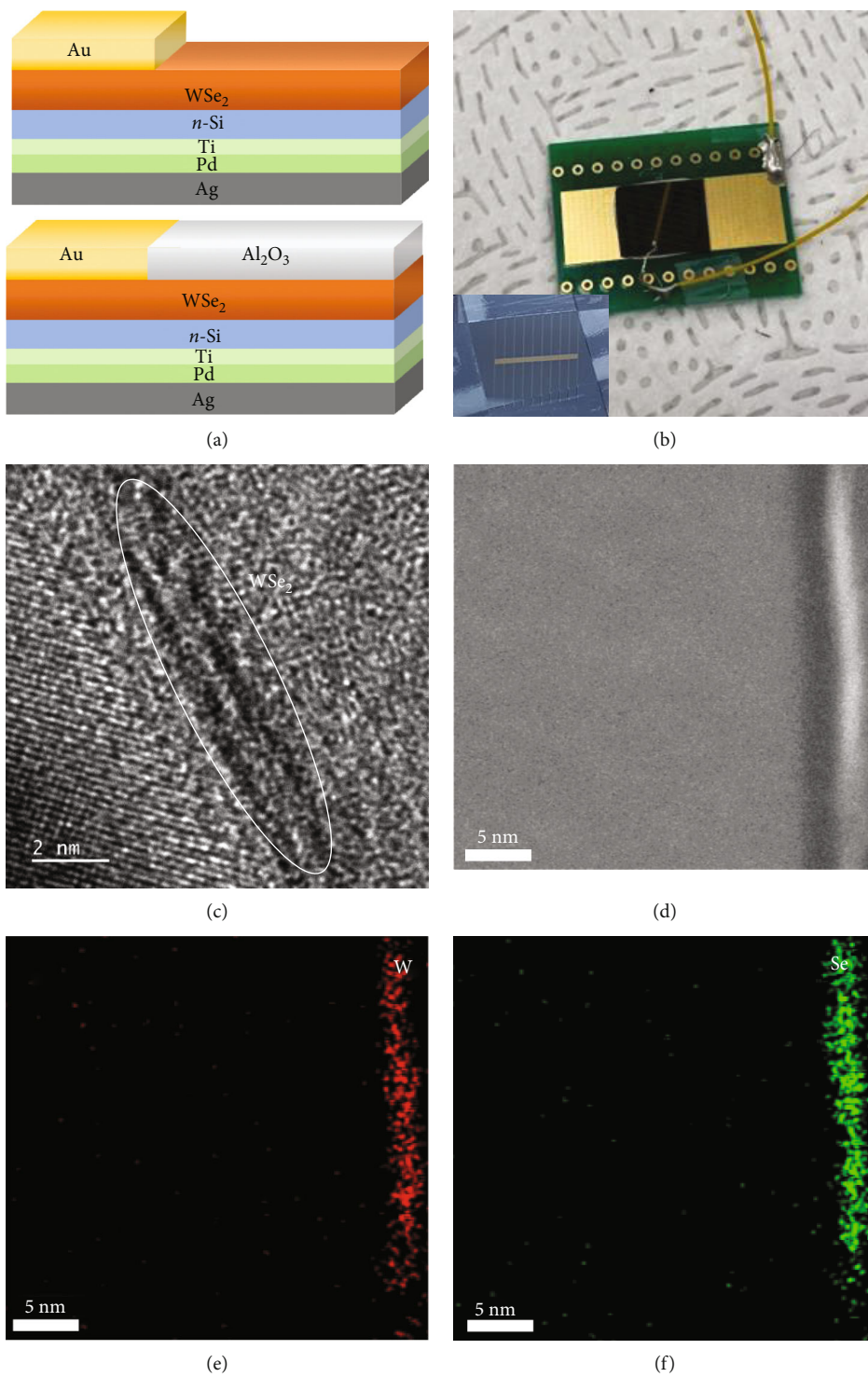
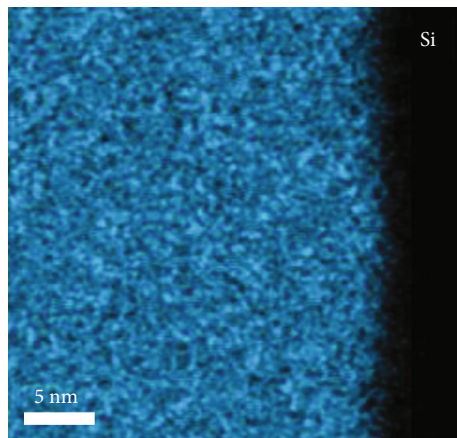


FIGURE 2: Continued.



(g)

FIGURE 2: (a) A schematic and (b) a photograph of the solar cell device structure. (c) A high-resolution TEM image, (d) a HAADF-STEM image, and (e) W, (f) Se, and (g) Si EDX elemental mapping images of the WSe₂/Si heterojunction.

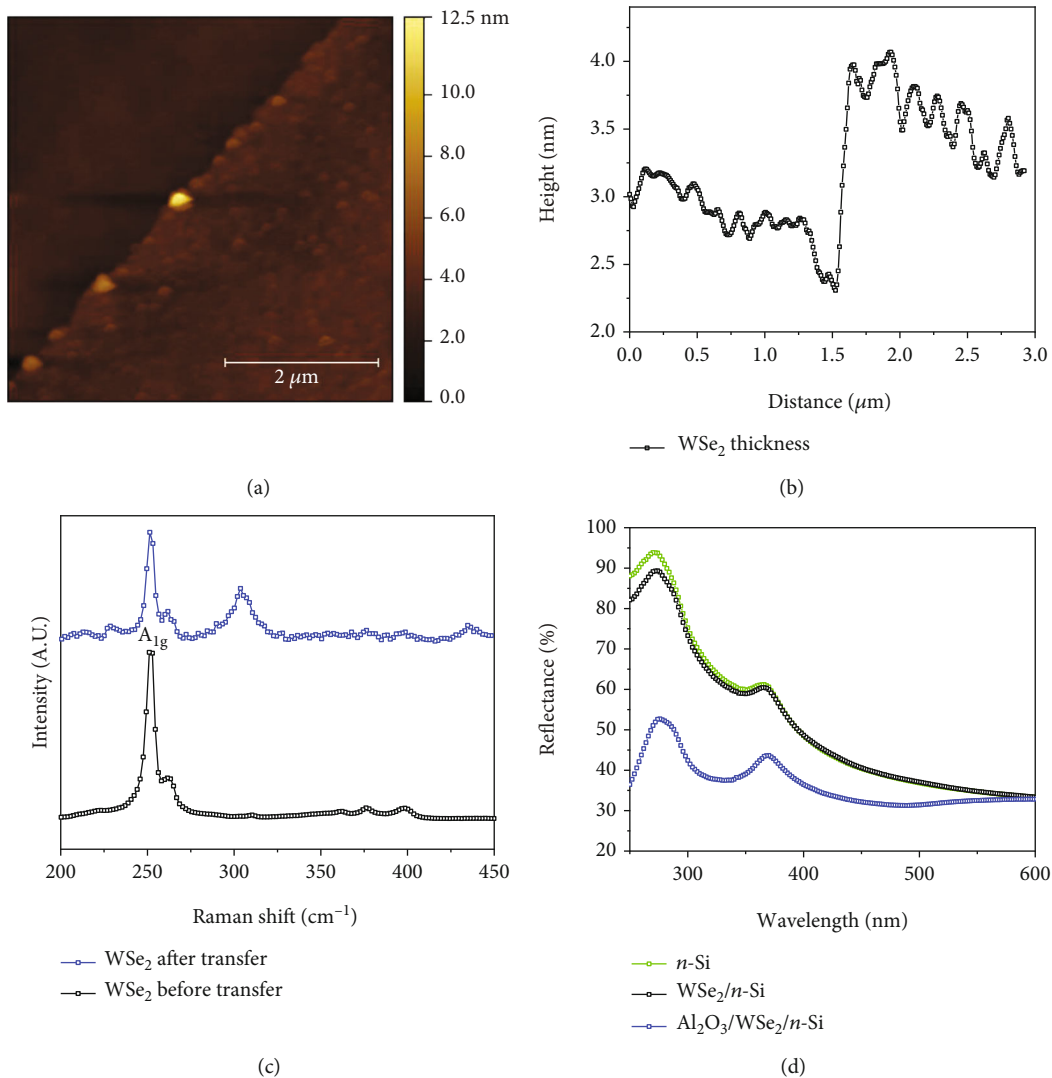


FIGURE 3: (a) An AFM image and (b) the corresponding height profile of CVD-grown WSe₂. (c) The Raman spectra of WSe₂ before and after transfer. (d) Reflectance measurements of *n*-type Si, WSe₂/*n*-type Si, and Al₂O₃/WSe₂/*n*-type Si.

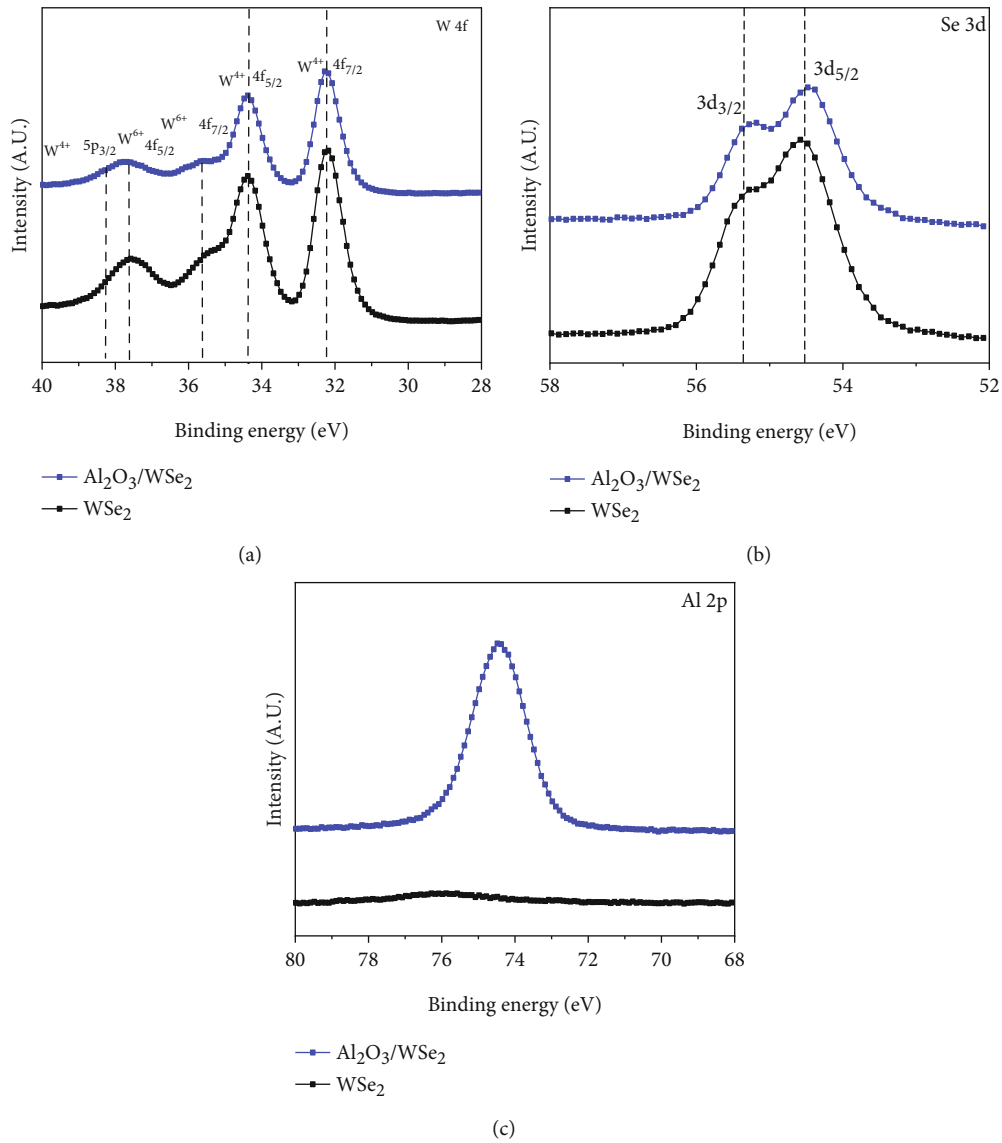


FIGURE 4: Deconvoluted (a) W 4f, (b) Se 3d, and (c) Al 2p XPS spectra for WSe_2 and $\text{Al}_2\text{O}_3/\text{WSe}_2$.

the binding energies for W $4f_{5/2}$ and W $4f_{7/2}$ (34.38 and 32.28 eV, respectively) were unchanged. However, the Se 3d XPS spectrum for $\text{Al}_2\text{O}_3/\text{WSe}_2$ shows that the binding energies of Se $3d_{3/2}$ and Se $3d_{5/2}$ (54.48 and 55.18 eV, respectively) had shifted slightly compared to pristine WSe_2 XPS. Moreover, the XPS Al 2p spectra in Figure 4(c) show that only the $\text{Al}_2\text{O}_3/\text{WSe}_2$ sample provided a peak with a binding energy of 74.48 eV due to the presence of Al_2O_3 [42].

We have built the band diagram which shows the band bending behavior of the p- WSe_2 and n-Si interface. This junction formed a type-II heterojunction (staggered gap) with a built-in potential that provoke tremendous photovoltaic performance in Figure 5(a). The EC, EV, and EF denote the energy levels for the bottom of the conduction band, the top of the valence band, and the Fermi level, respectively. The photovoltaic performance in this study was realized by using AM 1.5 solar light irra-

diation via a halogen lamp. The J-V curves for the $\text{WSe}_2/\text{n-type Si}$ and Al_2O_3 -passivated/ $\text{WSe}_2/\text{n-type Si}$ solar cells are shown in Figure 5(b). Upon irradiation, the short-circuit current density (J_{sc}) and V_{oc} were measured as indicators of the solar cell devices. The dark current curves for both devices confirm the rectifier property of the p-n junction diode, as shown in Figure 5(b). Compared to the $\text{WSe}_2/\text{n-type Si}$ solar cell, the J_{sc} of the Al_2O_3 -passivated $\text{WSe}_2/\text{n-type Si}$ solar cell increased from 9.25 to 19.12 mA/cm^2 and its V_{oc} increased from 0.25 to 0.66 V. The fill factor for the Al_2O_3 -passivated $\text{WSe}_2/\text{n-type Si}$ solar cell was 50% while its PCE compared to the $\text{WSe}_2/\text{n-type Si}$ solar cell was enhanced from 1.08% to 6.39%, which is the highest value obtained so far for a WSe_2 -based solar cell (Table 1). The device's active area in the current research was $0.6 \times 0.6 \text{ cm}^2$.

As well as being an antireflection coating, the passivating layer in solar cells is crucial because it safeguards the surface

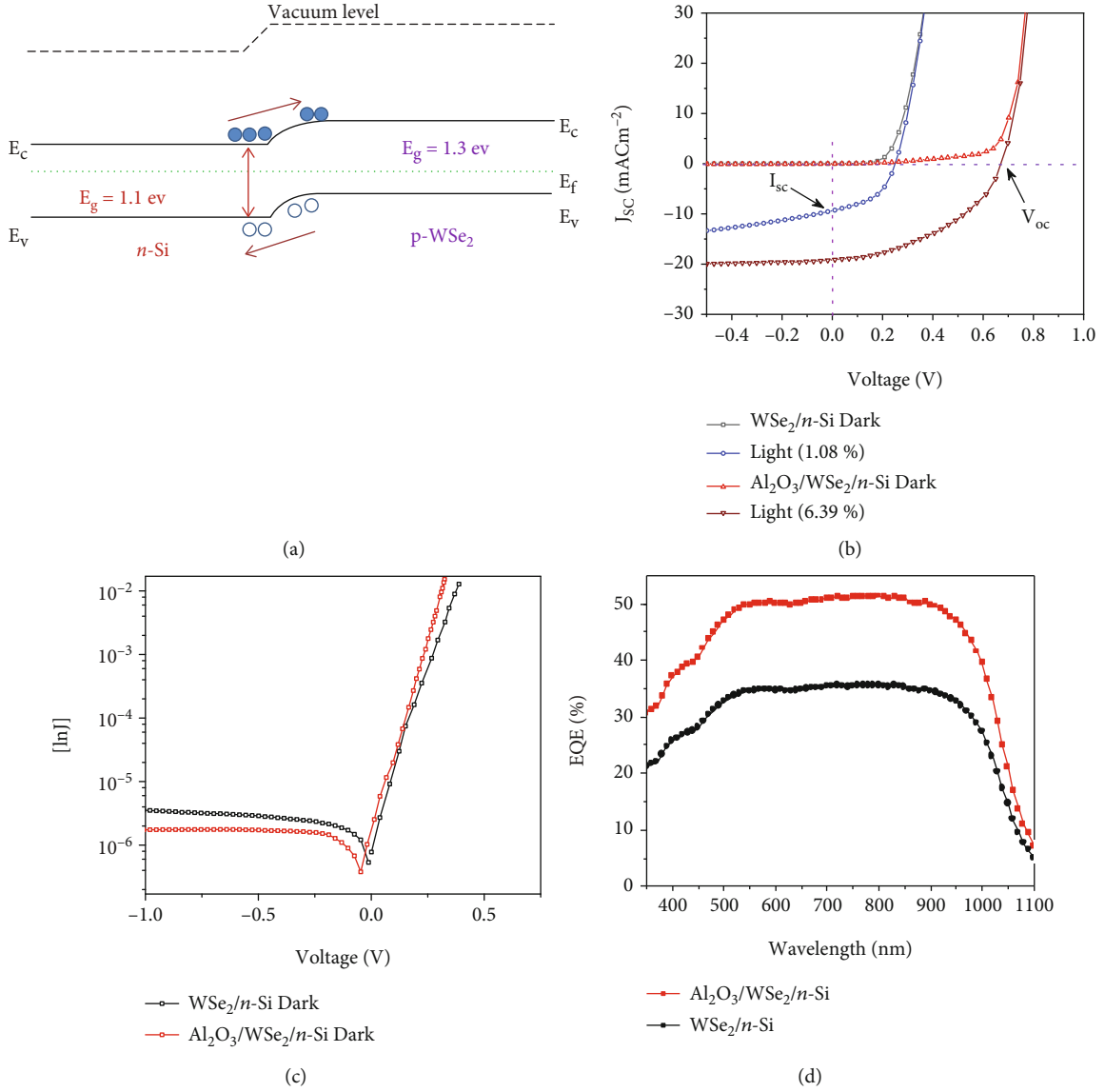


FIGURE 5: (a) The schematic representation of the energy-band diagram of the n -Si and p -WSe₂ heterostructure. Electrical characteristics of the WSe₂/ n -type Si and Al₂O₃/WSe₂/ n -type Si solar cells: (b) J-V curves, (c) ideality factor measurements, and (d) EQE plots.

TABLE 1: Comparison of the photovoltaic parameters of WSe₂-based solar cells.

Reference	Device structure	Applied strategy	Active area (cm ²)	V_{oc} (V)	J_{sc} (mA/cm ²)	Fill factor (%)	PCE (%)
[43]	ZnO/WSe ₂ /Mo	WSe ₂ /ZnO p-n junction	0.09	0.082	2.98	32	0.79
[44]	WSe ₂ /WS ₂	van der Waals heterojunction	1.74×10^{-6}	0.58	—	36	2.4
[45]	WSe ₂ / n -type Si	Nanosheet synthesize	0.04	0.34	1.55	55	2.91
[3]	WSe ₂ /Pt	—	1.8×10^{-5}	0.28	2.11	49	0.96
	Al ₂ O ₃ /WSe ₂ /Pt	Reflectance layers		0.36	2.43	58	1.7
This work	WSe ₂ / n -type Si	—	0.36	0.25	9.25	47	1.08
	Al ₂ O ₃ /WSe ₂ / n -type Si	Reflectance layers		0.66	19.12	50	6.39

V_{oc} : open-circuit voltage; J_{sc} : short-circuit current; PCE: power conversion efficiency.

by eliminating flaws and controlling the electric field profile. Passivation helps to enhance a device's performance and stability [22, 23]. Al_2O_3 as a passivating layer and an antireflection coating is a well-known strategy in semiconductor device studies [46–48].

There was a minor change in the dark current of the Al_2O_3 -passivated $\text{WSe}_2/\text{n-type Si}$ solar cell device, and the diode ideality factors of the $\text{WSe}_2/\text{n-type Si}$ solar cells with and without Al_2O_3 were 2.2 and 2.7, respectively (Figure 5(c)). These results indicate that bulk recombination processes were changed in the diode by passivation, which also suppressed the dark current. As can be seen from the solar cell parameter values, there were notable increases in both J_{sc} and V_{oc} due to Al_2O_3 passivation (from 9.25 to 19.12 mA/cm^2 and from 0.25 to 0.66 V, respectively). Overall, Al_2O_3 passivation improved the $\text{WSe}_2/\text{n-type Si}$ solar cell device performance through surface doping and trap passivation. To understand and quantify the conversion efficiency of incident photons at a certain wavelength, the external quantum efficiency (EQE) of the $\text{WSe}_2/\text{n-type Si}$ and $\text{Al}_2\text{O}_3/\text{WSe}_2/\text{n-type Si}$ devices was also evaluated in Figure 5(d). From the ultraviolet to the infrared regions, the $\text{WSe}_2/\text{n-type Si}$ and $\text{Al}_2\text{O}_3/\text{WSe}_2/\text{n-type Si}$ devices obtained EQEs of 35.3% and 51.2%, respectively. This is because the Al_2O_3 passivating layer reduced reflection and thus improved the EQE. Normally, the EQE is the measurement of the ratio between the numbers of charge carriers collecting the number of photon incident regardless of efficiency dependency. However, its current density should be similar to the current density obtained by solar measurement results. It gives evidence of accurate measured results. In our case, these are identical.

4. Conclusions

We successfully demonstrated the fabrication of a 2D $\text{WSe}_2/\text{n-type Si}$ heterojunction solar cell device involving a wet transfer process with TRT that is far simpler than the complicated lithography procedure. The realization of a $\text{WSe}_2/\text{n-type Si}$ heterojunction solar cell with Au fingers as the front contact and Ti/Pd/Ag as the bottom contact was achieved. The multilayered WSe_2 film provided an effective photovoltaic performance. Furthermore, surface doping and surface passivation with a coating of an Al_2O_3 passivating layer via ALD helped to enhance the PCE of the $\text{WSe}_2/\text{n-type Si}$ solar cell from 1.08% to 6.39%, which highlights the significance of surface passivation as well as an antireflection coating in TMDC-based solar cells. This work paves the way to realize TMDC-based solar cells with high PCEs by applying a facile cost-effective TRT approach as well as surface passivation through Al_2O_3 . This strategy could be utilized for other TMDCs in solar cells.

Data Availability

Data will be made available on request.

Conflicts of Interest

The authors declare that they have no conflicts of interest.

Authors' Contributions

Malik Abdul Rehman, Minjae Kim, and Sachin A. Pawar contributed equally to this work.

Acknowledgments

This work was supported by the National Research Foundation of Korea (NRF) grant funded by the Korean Government (grant number: 2019R1A2C2087604) and the Creative Materials Discovery Program through the National Research Foundation of Korea funded by the Ministry of Science and ICT (grant number: 2018M3D1A1058536).

References

- [1] J. H. Park, D. Kim, S. S. Shin et al., "Van der Waals heterojunction interface passivation using ZnS nanolayer and enhanced photovoltaic behavior of semitransparent ultrathin 2D-MoS₂/3D-chalcogenide solar cells," *Applied Surface Science*, vol. 558, article 149844, 2021.
- [2] Y. Zhao, L. Yu, and M. Sun, "Recent progress in emerging 2D layered materials for organic solar cells," *Solar Energy*, vol. 218, pp. 621–638, 2021.
- [3] E. McVay, A. Zubair, Y. Lin, A. Nourbakhsh, and T. Palacios, "Impact of Al_2O_3 passivation on the photovoltaic performance of vertical WSe_2 Schottky junction solar cells," *ACS Applied Materials & Interfaces*, vol. 12, no. 52, pp. 57987–57995, 2020.
- [4] R. Chaurasiya, G. K. Gupta, and A. Dixit, "Heterostructure AZO/WSeTe/W(S/Se)₂ as an efficient single junction solar cell with ultrathin Janus WSeTe buffer layer," *Journal of Physical Chemistry C*, vol. 125, no. 8, pp. 4355–4362, 2021.
- [5] S. Rashidi, S. Rashidi, R. K. Heydari et al., "WS₂ and MoS₂ counter electrode materials for dye-sensitized solar cells," *Progress in Photovoltaics: Research and Applications*, vol. 29, no. 2, pp. 238–261, 2021.
- [6] K. H. Kim, M. Andreev, S. Choi et al., "High-efficiency WSe_2 -Photovoltaic devices with electron-selective contacts," *ACS Nano*, vol. 16, no. 6, pp. 8827–8836, 2022.
- [7] W. S. Yun, S. W. Han, S. C. Hong, I. G. Kim, and J. D. Lee, "Thickness and strain effects on electronic structures of transition metal dichalcogenides: 2H-MX₂ semiconductors (M = Mo, W; X = S, Se, Te)," *Physical Review B*, vol. 85, no. 3, article 033305, 2012.
- [8] W. Zhao, Z. Ghorannevis, L. Chu et al., "Evolution of electronic structure in atomically thin sheets of WS₂ and WSe₂," *ACS Nano*, vol. 7, no. 1, pp. 791–797, 2013.
- [9] A. Splendiani, L. Sun, Y. Zhang et al., "Emerging photoluminescence in monolayer MoS₂," *Nano Letters*, vol. 10, no. 4, pp. 1271–1275, 2010.
- [10] K. F. Mak, C. Lee, J. Hone, J. Shan, and T. F. Heinz, "Atomically thin MoS₂: a new direct-gap semiconductor," *Physical Review Letters*, vol. 105, no. 13, article 136805, 2010.
- [11] S. A. Pawar, D. Kim, R. Lee et al., "Efficient supercapacitor based on polymorphic structure of 1T''-Mo₆Te₆ nanoplates and few-atomic-layered 2H-MoTe₂: a layer by layer study on

- nickel foam,” *Chemical Engineering Journal*, vol. 371, pp. 182–192, 2019.
- [12] C. Hou, C. Huang, H. Yu, and S. Shi, “Surface-engineered $Ti_3C_2T_x$ with tunable work functions for highly efficient polymer solar cells,” *Small*, vol. 18, no. 21, article 2201046, 2022.
- [13] J. Zhang, C. Huang, Y. Sun, and H. Yu, “Amino-functionalized niobium-carbide MXene serving as electron transport layer and perovskite additive for the preparation of high-performance and stable methylammonium-free perovskite solar cells,” *Advanced Functional Materials*, vol. 32, no. 24, article 2113367, 2022.
- [14] M. Shimasaki, T. Nishihara, K. Matsuda et al., “Directional exciton-energy transport in a lateral heteromonolayer of WSe_2 - $MoSe_2$,” *ACS Nano*, vol. 16, no. 5, pp. 8205–8212, 2022.
- [15] Y. Huang, X. Shi, X. Liu et al., “Boosting the photovoltaic performance of MoS_2/Si heterojunction solar cells with thiourea-doped MoS_2 films,” *Micro and Nanostructures*, vol. 167, article 207241, 2022.
- [16] F. Wu, H. Li, L. Yao et al., “In-situ hydrothermal growth of MoS_2 absorber layer for planar heterojunction solar cells,” *Solar Energy*, vol. 230, pp. 754–763, 2021.
- [17] A. J. Cho and J. Y. Kwon, “Hexagonal boron nitride for surface passivation of two-dimensional van der Waals heterojunction solar cells,” *ACS Applied Materials & Interfaces*, vol. 11, no. 43, pp. 39765–39771, 2019.
- [18] A. J. Cho, M. K. Song, D. W. Kang, and J. Y. Kwon, “Two-dimensional WSe_2/MoS_2 p-n heterojunction-based transparent photovoltaic cell and its performance enhancement by fluoropolymer passivation,” *ACS Applied Materials & Interfaces*, vol. 10, no. 42, pp. 35972–35977, 2018.
- [19] W. Liu, J. Kang, D. Sarkar, Y. Khatami, D. Jena, and K. Banerjee, “Role of metal contacts in designing high-performance monolayer n-type WSe_2 field effect transistors,” *Nano Letters*, vol. 13, no. 5, pp. 1983–1990, 2013.
- [20] W. Liu, W. Cao, J. Kang, and K. Banerjee, “(Invited) high-performance field-effect-transistors on monolayer- WSe_2 ,” *ECS Transactions*, vol. 58, no. 7, pp. 281–285, 2013.
- [21] C. M. Went, J. Wong, P. R. Jahlka et al., “A new metal transfer process for van der Waals contacts to vertical Schottky-junction transition metal dichalcogenide photovoltaics,” *Science Advances*, vol. 5, no. 12, article eaax6061, 2019.
- [22] S. Wi, M. Chen, D. Li, H. Nam, E. Meyhofer, and X. Liang, “Photovoltaic response in pristine WSe_2 layers modulated by metal-induced surface-charge-transfer doping,” *Applied Physics Letters*, vol. 107, no. 6, article 062102, 2015.
- [23] D. Jariwala, A. R. Davoyan, J. Wong, and H. A. Atwater, “Van der Waals materials for atomically-thin photovoltaics: promise and outlook,” *ACS Photonics*, vol. 4, no. 12, pp. 2962–2970, 2017.
- [24] P. Saint-Cast, J. Benick, D. Kania et al., “High-efficiency c-Si solar cells passivated with ALD and PECVD aluminum oxide,” *IEEE Electron Device Letters*, vol. 31, no. 7, pp. 695–697, 2010.
- [25] G. Dingemans, R. Seguin, P. Engelhart, M. C. M. van de Sanden, and W. M. M. Kessels, “Silicon surface passivation by ultrathin Al_2O_3 films synthesized by thermal and plasma atomic layer deposition,” *Physica Status Solidi Rapid Research Letters*, vol. 4, no. 1-2, pp. 10–12, 2010.
- [26] A. U. Rehman, M. F. Khan, M. A. Shehzad et al., “N- MoS_2/p -Si Solar cells with Al_2O_3 passivation for enhanced photogeneration,” *ACS Applied Materials & Interfaces*, vol. 8, no. 43, pp. 29383–29390, 2016.
- [27] A. J. Cho, S. Yang, K. Park, S. D. Namgung, H. Kim, and J. Y. Kwon, “Multi-layer MoS_2 FET with small hysteresis by using atomic layer deposition Al_2O_3 as gate insulator,” *ECS Solid State Letters*, vol. 3, no. 10, pp. Q67–Q69, 2014.
- [28] M. F. Khan, G. Nazir, V. M. Lermolenko, and J. Eom, “Electrical and photo-electrical properties of MoS_2 nanosheets with and without an Al_2O_3 capping layer under various environmental conditions,” *Science and Technology of Advanced Materials*, vol. 17, no. 1, pp. 166–176, 2016.
- [29] J. Na, M. K. Joo, M. Shin et al., “Low-frequency noise in multilayer MoS_2 field-effect transistors: the effect of high-k passivation,” *Nanoscale*, vol. 6, no. 1, pp. 433–441, 2014.
- [30] G. Wu, X. Wang, Y. Chen et al., “ $MoTe_2p$ -n homojunctions defined by ferroelectric polarization,” *Advanced Materials*, vol. 32, no. 16, article 1907937, 2020.
- [31] A. Choi, A. T. Hoang, T. T. N. Van et al., “Residue-free photolithographic patterning of graphene,” *Chemical Engineering Journal*, vol. 429, article 132504, 2022.
- [32] J. Potschavage, A. Sharma, and B. Kippelen, “Critical interfaces in organic solar cells and their influence on the open-circuit voltage,” *Accounts of Chemical Research*, vol. 42, no. 11, pp. 1758–1767, 2009.
- [33] C. J. Brabec, A. Cravino, D. Meissner et al., “Origin of the open circuit voltage of plastic solar cells,” *Advanced Functional Materials*, vol. 11, no. 5, pp. 374–380, 2001.
- [34] L. Favereau, Y. Pellegrin, L. Hirsch et al., “Engineering processes at the interface of p-semiconductor for enhancing the open circuit voltage in p-type dye-sensitized solar cells,” *Advanced Energy Materials*, vol. 7, no. 12, article 1601776, 2017.
- [35] Y. Jang, Y. M. Seo, H. S. Jang, K. Heo, and D. Whang, “Performance improvement of residue-free graphene field-effect transistor using Au-assisted transfer method,” *Sensors*, vol. 21, no. 21, p. 7262, 2021.
- [36] S. Hussain, S. A. Patil, D. Vikraman et al., “Growth of a WSe_2/W counter electrode by sputtering and selenization annealing for high-efficiency dye-sensitized solar cells,” *Applied Surface Science*, vol. 406, pp. 84–90, 2017.
- [37] D. G. Mead and J. C. Irwin, “Long wavelength optic phonons in WSe_2 ,” *Canadian Journal of Physics*, vol. 55, pp. 379–382, 1977.
- [38] H. Zeng, G. Bin Liu, J. Dai et al., “Optical signature of symmetry variations and spin-valley coupling in atomically thin tungsten dichalcogenides,” *Scientific Reports*, vol. 3, 2013.
- [39] Y. Ma, B. Liu, A. Zhang et al., “Reversible semiconducting-to-metallic phase transition in chemical vapor deposition grown monolayer WSe_2 and applications for devices,” *ACS Nano*, vol. 9, no. 7, pp. 7383–7391, 2015.
- [40] H. Li, G. Lu, Y. Wang et al., “Mechanical exfoliation and characterization of single- and few-layer nanosheets of WSe_2 , TaS_2 , and $TaSe_2$,” *Small*, vol. 9, no. 11, pp. 1974–1981, 2013.
- [41] A. Ambrosi, Z. Sofer, and M. Pumera, “ $2H \rightarrow 1T$ phase transition and hydrogen evolution activity of MoS_2 , $MoSe_2$, WS_2 and WSe_2 strongly depends on the MX_2 composition,” *Chemical Communications*, vol. 51, no. 40, pp. 8450–8453, 2015.
- [42] T. Tago, N. Kataoka, H. Tanaka, K. Kinoshita, and S. Kishida, “XPS study from a clean surface of Al_2O_3 single crystals,” *Procedia Engineering*, vol. 216, pp. 175–181, 2017.
- [43] X. Mao, J. Zou, H. Li, Z. Song, and S. He, “Magnetron sputtering fabrication and photoelectric properties of WSe_2 film solar cell device,” *Applied Surface Science*, vol. 444, pp. 126–132, 2018.

- [44] P. Lin and J. Yang, "Tunable WSe₂/WS₂ van der Waals hetero-junction for self-powered photodetector and photovoltaics," *Journal of Alloys and Compounds*, vol. 842, article 155890, 2020.
- [45] P. M. Pataniya, C. K. Zankat, M. Tannarana et al., "Photovoltaic activity of WSe₂/Si hetero junction," *Materials Research Bulletin*, vol. 120, article 110602, 2019.
- [46] L. Yu, A. Zubair, E. J. G. Santos et al., "High-performance WSe₂ complementary metal oxide semiconductor technology and integrated circuits," *Nano Letters*, vol. 15, no. 8, pp. 4928–4934, 2015.
- [47] S. Yang, J. Cha, J. C. Kim et al., "Monolithic interface contact engineering to boost optoelectronic performances of 2D semiconductor photovoltaic heterojunctions," *Nano Letters*, vol. 20, no. 4, pp. 2443–2451, 2020.
- [48] D. Kufer and G. Konstantatos, "Highly sensitive, encapsulated MoS₂ photodetector with gate controllable gain and speed," *Nano Letters*, vol. 15, no. 11, pp. 7307–7313, 2015.